IEEE Access
Multidisciplinary | Rapid Review | Open Access Journal

Received March 24, 2022, accepted May 27, 2022, date of publication June 14, 2022, date of current version June 24, 2022.

Digital Object Identifier 10.1109/ACCESS.2022.3183152

Investigation of Ionospheric Effects in the Planning of the AlfaCrux UHF Satellite Communication System

A. A. FERREIRA[1,2], (Member, IEEE), R. A. BORGES[2], (Senior Member, IEEE), L. R. REIS[2], C. BORRIES[1], AND D. VASYLYEV[1]

[1]German Aerospace Center, Institute for Solar-Terrestrial Physics, 17235 Neustrelitz, Germany
[2]Department of Electrical Engineering, University of Brasília, Campus Darcy Ribeiro, Brasília 70910-900, Brazil

Corresponding author: A. A. Ferreira (arthur.ferreira@dlr.de)

ABSTRACT Recent technological advances and new launch opportunities have allowed the development and spread of small satellite missions for commercial and educational purposes and different applications. Among this category of small satellites, CubeSats have attracted lots of attention given their low design-and-deployment costs. Such satellites usually operate in the narrow ranges of the UHF frequency band to perform the communication activities. Although it provides lower data rate, the use of narrowband can be advantageous when compared to broadband, due to its better penetration and lower attenuation in the troposphere. However, the signals in this frequency band can be significantly affected by the ionosphere. This work investigates the ionospheric effects, namely the Faraday rotation and scintillation, on the UHF satellite communication systems, taking as a case study the AlfaCrux CubeSat mission, which is an 1U CubeSat mission planned for conducting research activities in the field of satellite-mediated communication. In particular, we investigate the variability of Faraday rotation and amplitude scintillation with the daytime, season, and geographic position for periods of low and high solar activity. In addition, this work presents a methodology of risk estimation for communication outage over the Brazilian sector. Aiming to address the most realistic communication scenario, we include in this analysis the effects due to scintillation, free-space propagation, tropospheric attenuation, and polarization losses. By doing so, the regions with the high risk of communication outage may be estimated in advance and used for optimal mission planning.

INDEX TERMS CubeSat, faraday rotation, ionospheric scintillation, UHF satellite communication.

I. INTRODUCTION

A small satellite is a spacecraft built at relatively low cost, which is able to serve not only to education purposes, but also space services and applications. Among the small satellites category, the CubeSat has appeared as a good opportunity for universities to approach space research. They are intended to be built in a short time frame, at relatively low cost, and they make significant use of state-of-the-art commercial-of-the-shelf (COTS) technologies [1].

The CubeSat standard was developed by the California Polytechnic State University (CalPoly) and the Space Systems Development Laboratory of Stanford University. The term *CubeSat*, refers to a category of small satellites built in a modular fashion and have as a basic unity a cube of dimensions 10 cm × 10 cm × 10 cm with the mass up to 1.33 kg. This basic unity is also called the CubeSat Unity (1U) [2]. These modules can be combined to form CubeSats in different sizes (1U, 2U, 3U and 6U) that can be launched as a secondary payload reducing the launching costs and allowing universities to conduct space science experimentation [2], [3]. A CubeSat mission may consist of only one single satellite operated individually or it can contain a cluster/swarm of CubeSats. In the former case, a CubeSat collects data for specific scientific experiments, performs basic data processing and transmits these data via a radio transceiver to a ground station, where these data are further processed and analyzed. In the latter case, satellites may establish inter-satellite communication links and share the collected scientific data along with the ancillary data (such as positioning and timing), allowing the satellites of the cluster to perform a joint/distributed processing of data [2].

The associate editor coordinating the review of this manuscript and approving it for publication was Venkata Ratnam Devanaboyina.

In this framework, the AlfaCrux mission conducted by the University of Brasília (UnB) is proposed as an educational and technological demonstration mission in the area of CubeSat telecommunication. The aim of the mission is to provide a hands-on experience to the team members in the complete process of developing and operating a space mission to provide a narrowband communication solution to exchange data between ground and space segments, enabling, for instance, data network in remote areas with limited infrastructure. A preliminary overview and concept of operation can be seen in [4].

In order to accomplish these objectives, the mission is planned to operate on a narrowband, more specifically, on the ultra-high-frequency (UHF) radio amateur band. In the context of satellite communications, the term *narrowband* (NB) refers to the UHF-, L- and S-bands, where the bandwidth is limited. The lower frequency bands (300 MHz to 4 GHz) can be advantageous when compared to the higher frequency bands due to their better penetration into buildings, foliage and due to their lower level of attenuation in adverse weather conditions [5]. These pros are important when trying to establish a satellite communication link in areas of tropical forest, such as the Amazon regions, which are characterized by a considerably dense foliage, and high level of humidity [4].

Although advantageous in the aforementioned situations, the narrowband satellite communication (SATCOM) has the disadvantage of providing low-rate data transfer, due to the limited bandwidth. Besides that, trans-ionospheric signals transmitted in these bands are more susceptible to the effects of the ionosphere. Brazil is located in the low latitudes, a region with different strong ionosphere effects like the equatorial ionization anomaly [6], ionospheric plasma bubbles and irregularities [7]. Considering these conditions, the ionospheric impact on the AlfaCrux's signal propagation has to be treated carefully during the mission design. In its Low-Earth Orbit (LEO), the satellite will have up to five contacts per day with less than 12 minutes duration each [8]. Due to these scarce opportunities for signal transmission, the understanding of the ionosphere impact on the signal propagation is essential for the planning and efficient use of the communication channel. In this context, this work proposes a new methodology to assess the risk of communication outage due to ionospheric scintillation.

The proposed methodology is of great importance for the mission planning and considers realistic communication scenarios. In order to retrieve ionospheric scintillation information, we make use of an already validated climatological scintillation model. Although such climatological model is not able to reproduce some transient events due to geomagnetic storms, it has the advantages of allowing the investigation of different frequencies and providing good spatial coverage.

This paper is organized as follows. In Section II we describe the Faraday rotation and ionospheric scintillation phenomena, together with their morphology over the Brazilian sector for quiet and disturbed space weather conditions. Section III presents the impact of ionospheric scintillation on the communication and proposes a methodology to estimate the risk of communication outage due to the associated fluctuating losses and due to the deterministic losses along the communication link. A summary and discussion are given in Sec. IV.

II. SPACE WEATHER IMPACT ON UHF COMMUNICATION

Investigations of space weather effects on modern technological systems have significantly increased during the last decades, given the impact these events can have over such systems [9]. Space weather has important effects on technologies operating at UHF band, such as radars and satellite based communications in regions of scintillation [10]. Considering the purpose and characteristics of the AlfaCrux mission, two effects of the ionosphere on the communication channel are investigated in this work: the Faraday rotation (FR) and the ionospheric scintillation. The impact of such effects on the mission and the proposed approaches to deal with them are presented in the next sections.

A. FARADAY ROTATION

The antennas installed in the CubeSats can be either linearly or circularly polarized. In case of linearly polarized antennas, keeping the polarization of the signal across the propagation path is crucial in order to ensure its reception. In this regard, the major problems in matching the transmitter and receiver antenna polarizations occur due to ionospheric effects, more specifically due to the Faraday rotation [11]. This effect corresponds to a rotation of the polarization plane of linearly polarized radio-waves propagating in the ionospheric medium and exposed to the action of the geomagnetic field. The FR is inversely proportional to the squared frequency of the signal and may impact different applications (e.g. spaceborne synthetic aperture radar (SAR) systems, and microwave radiometers) [12], [13].

In addition to the frequency, the geomagnetic field and the electron density in the ionosphere are the geophysical quantities that influence the magnitude of the FR angle. This effect can be expressed as [13]–[15]:

$$FR[radians] = \frac{e^3}{8\pi^2 m^2 c \varepsilon_0 f^2} \int N_e B \cos\psi \, ds, \qquad (1)$$

where c is the free-space velocity of light, e is the electron charge, m is the electron mass, ε_0 is the permittivity of free space, f is the frequency of the signal, N_e is the electron density, B is the magnetic field. The angle ψ is the angle between the electromagnetic wave vector and earth's magnetic field vector.

The integration in (1) is performed along the propagation path with line element ds. The calculations of the FR can be simplified if one neglect the finiteness of the earth or ionospheric shell curvatures. Additionally to this, we neglect the refractive bending of the signal ray at high zenith angles, θ_o, of a ground-based receiver (nadir angles of the

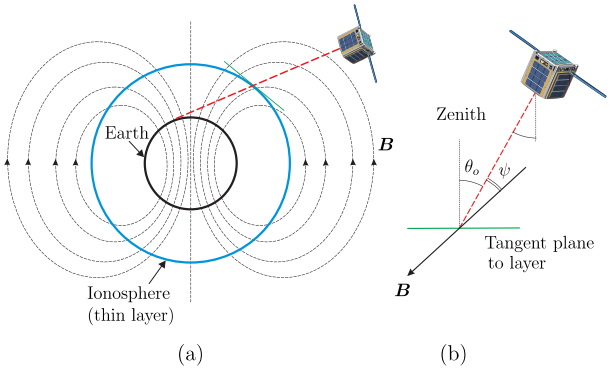

FIGURE 1. Communication schematics with a CubeSat satellite (a). Under the assumption of small zenith angle θ_o of the receiver, the geometry presented in (b) can be applied for the derivation of (2). Here the zenith angle θ_o is constant along the communication link and it is assumed that the angle ψ is formed between the signal propagation direction and the direction of the magnetic field B.

communication satellite). One can express the slant path element in (1) as $ds = \sec\theta_o dh$. Here dh is the corresponding vertical line and the integration can be performed from altitude of the ground station, $h_r = 0$, up to the satellite altitude h_s [15].

Further simplification of (1) is obtained if it is assumed that the external magnetic field B is constant. In this case, the angle of rotation is proportional to $\int N_e dh$, i.e., to the total electron content (TEC). Equation (1) can be approximated as:

$$FR[radians] = \frac{K}{f^2} \cdot B\cos\psi \sec\theta_0 \cdot TEC, \qquad (2)$$

where the magnetic field factor K is obtained considering a constant height of 400 km, cf. Ref. [15] and K is a constant of value $2.365 \times 10^4 [\mathrm{A}\cdot\mathrm{m}^2/\mathrm{kg}]$ in S.I. units.

1) VARIABILITY OF FARADAY ROTATION EFFECT

For investigation of the temporal and seasonal variability of the FR, we have chosen the coordinates of Brasília, Brazil (15° 48′ S, 47° 51′ W) and analyzed the FR effect for the years of 2015 and 2018. These years correspond to maximum and minimum periods of the solar cycle 24, respectively. The purpose of choosing two different periods is to illustrate the contribution of the solar cycle on the FR variation.

In order to account for the attenuation due to the polarization effects, we also consider the polarization loss factor (PLF) given by $\mathrm{PLF} = \cos^2\theta$, where θ is the angle between the polarization vectors of the signal and the receiver [16]. A PLF equals to zero corresponds to a complete misalignment of polarization planes of the sent and received signal. Fig. 2, upper panel, presents the results for the year of 2015. One can note clear seasonal and daily variability of the polarization loss factor. During the whole year it is observed a decreasing on the PLF on the afternoon-night hours (from around noon to 2:00 LT) from January to May and from October to December, indicating that during these periods a higher signal attenuation due to the depolarization

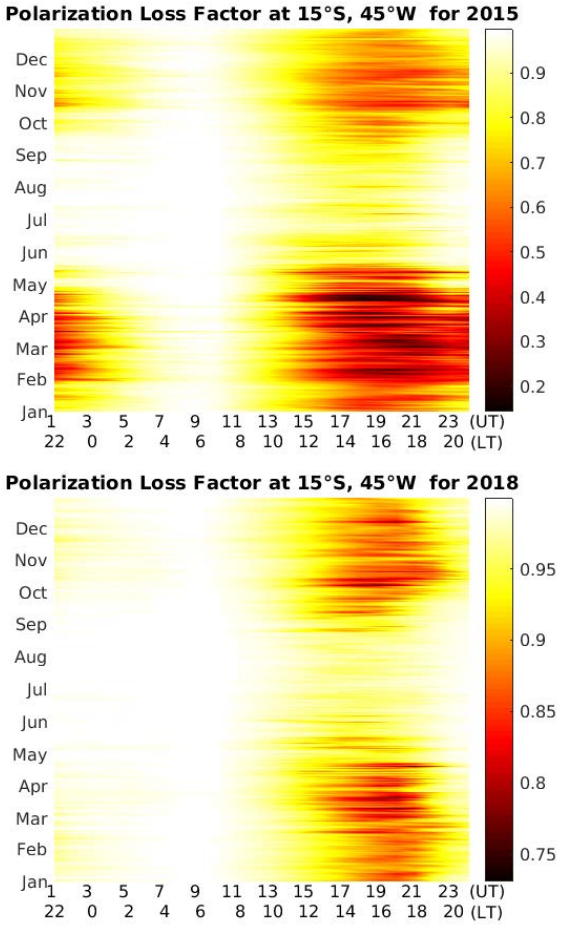

FIGURE 2. Polarization loss factor at 15°S and 45°W for 2015 (upper panel) and 2018 (lower panel).

is expected. From June to September, on the other hand, one can note a high PLF during the whole day, indicating that for this time of the year (which corresponds to the winter in the Brazilian region), a reduced attenuation due to the depolarization is expected.

In addition to this, one can note that the two periods of low PLF values (January to May and October to December) do not exhibit the same magnitude, with the first period having more impact on the signal attenuation than the second one. This might be related to the variation due to the solar cycle, which can lead to a lower level of ionization and, consequently, to a lower attenuation due to the FR effect.

Fig. 2, lower panel, shows the PLF for the year 2018. As mentioned above, the year 2018 corresponds to a minimum of the solar cycle 24, and as a consequence, one can expect a lower level of ionization of the ionosphere. By comparing both panels on Fig. 2 one can clearly note a significant difference on the magnitude of the PLF. Although there are two peaks of low PLF in 2018 (from January to May and October to December, in the similar way as they appear in 2015), in this case the PLF does not reach values below 0.75. This means that the impact of the ionosphere on polarization

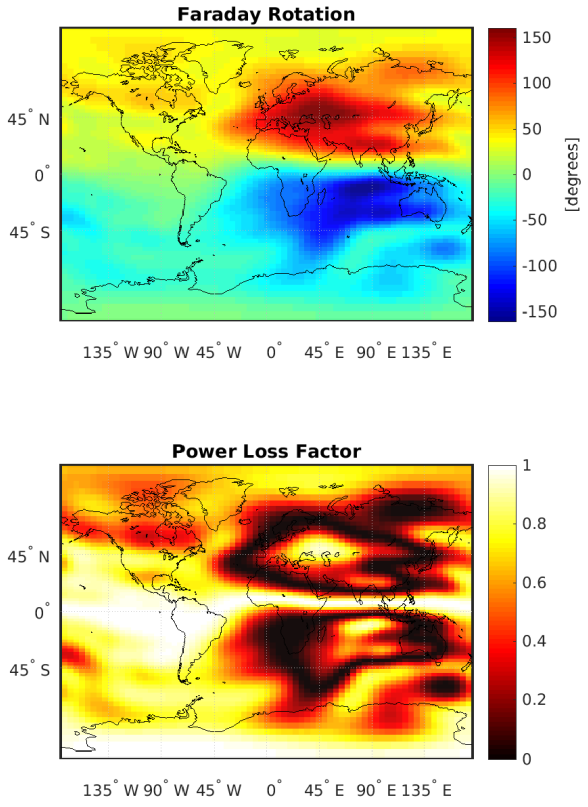

FIGURE 3. Upper panel: Faraday rotation at 12 UT for a 437 MHz signal frequency for St. Patrick's day storm (March 17, 2015), Lower panel: PLF associated with the FR presented in the upper panel.

is less severe for the year 2018 during the solar minimum in comparison to the year 2015 of the solar maximum. Also, the lower PLF values are concentrated in a considerably shorter interval (from around 12:00 until 20:00 LT).

The median value of the Faraday rotation exhibits regular diurnal, seasonal and solar cyclical variations that can be predicted and, therefore, compensated by a manual adjustment of the polarization tilt angle at the ground station antennas. However, this regular behaviour can be significantly changed as a result of space weather events, such as Storm Enhanced Densities (SED) and Travelling Ionospheric Disturbances (TIDs) [17]. Also, intermittent changes of FR angles of very-high frequency (VHF) signals have been associated with strong and fast scintillation occurring at locations near the crests of the Equatorial Ionization Anomaly [18]. To analyze and illustrate this influence, we have chosen a geomagnetic event that occurred in the maximum phase of the solar cycle 24.

Fig. 3 presents the FR and the PLF for the St. Patrick's day geomagnetic storm that took place on March 17, 2015. This event occurred during a solar maximum period and lead to significant FR levels. The maximum solar radio flux registered for this storm was around 138 solar flux units (sfu). The FR and PLF values are shown for a linearly polarized signal propagating in vertical direction to the ground ($\theta_o = 0$). As presented in Fig. 3, lower panel, the polarization orientation may change to the orthogonal one for some regions of the globe. Hence, in these regions the communication can be completely interrupted if the linearly polarized receiver antennas are used.

TABLE 1. Elements of the TLE used for the orbit calculations. Some parameters, such as the epoch, have been adjusted to correspond to the time of ionospheric conditions considered in the article.

Parameter	Value
Epoch	17241.99979167
Inclination	97.0000 (degrees)
RAAN	153.1430 (degrees)
Eccentricity	0.0003134
Argument of perigee	220.5360 (degrees)
Mean anomaly	108.0034 (degrees)
Mean motion	15.13104507 (revolutions per day)

2) FARADAY ROTATION FOR SLANT PROPAGATION PATHS

Previously we have considered primarily the situations when the signal approaches the ground receiver from near zenith direction. For example, Fig. 3 is calculated for the case of vertical propagation of the signal ($\theta_o = 0$). For the zenith angles in the range $\theta_o \in [0°, 60°]$, one can use (2) to estimate the FR for slant propagation paths. However, for higher values of the zenith angle one should account for the refractive bending of the signal radio rays caused by the ionospheric layer. Thus, one should use the general formula (1) along with the proper ray-tracing algorithm for calculation of the bent propagation paths.

We visualize the FR angle for slant communication links by mapping the calculated values on the sky plot for specified ground receiving stations. In this article we consider four GNSS receiver ground stations located in Brazil, namely BOAV (Boa Vista, 2°50′ N, 60°42′ W), BRAS (Brasília, 15° 47′ S, 47° 52′ W), CUIB (Cuiabá, 15°33′ S, 56°04′ W), and SALU (São Luís, 2°35′ S, 44° 12′ W). Fig. 4, upper panel, shows the geographical locations of these stations together with possible ground tracks of the AlfaCrux satellite, whose instantaneous position is marked by a dot. The satellite trajectory has been calculated with the Keplerian elements adjusted to the parameters of the planned mission.

Table 1 summarizes the principal orbit information included in the corresponding sample Two Lines Elements (TLE) used in the calculation. The mapped satellite trajectories serve for illustrative purpose of possible communication scenarios.

Fig. 4, lower panel, shows the FR angle calculated using the Global Ionospheric Scintillation Model (GISM) [19], [20] for the BOAV station for the 7th of September 2017 at 01:30 UT. The GISM has the capability to calculate the FR for arbitrary communication links with the inclusion of ray bending effects. One can see that the FR is small for small and moderate zenith angles, but it can reach values greater than one radian when approaching the large zenith angles. In particular, for the considered time and geographic location,

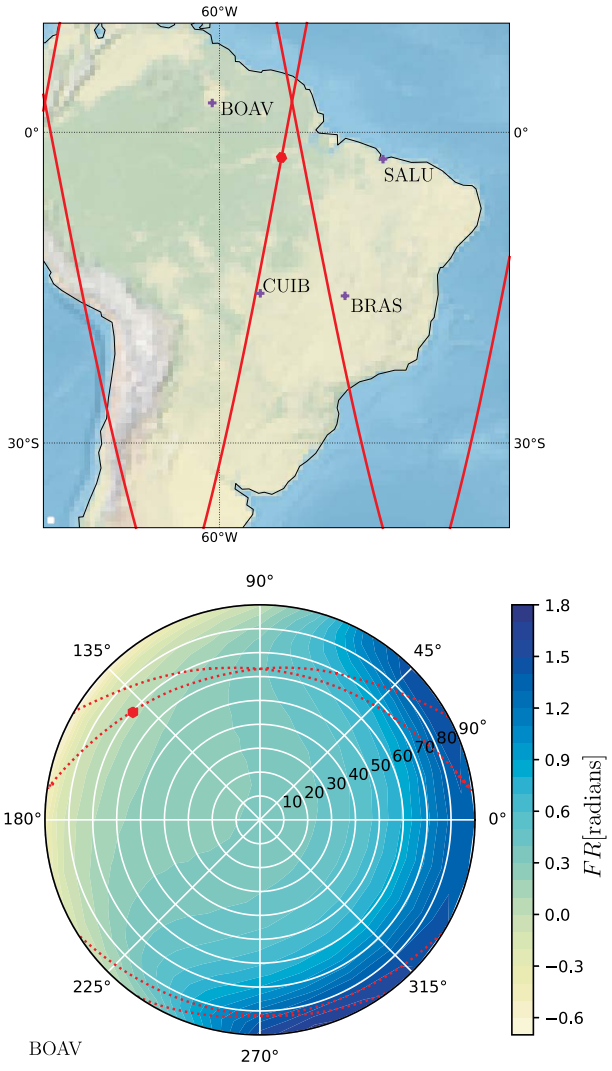

FIGURE 4. Upper panel: locations of the ground stations BOAV, BRAS, CUIB, and SALU. The possible trajectories of the communication satellite calculated using the Keplerian elements from Table 1. The instantaneous position of the satellite at 01:30 UT, 7th of September 2017, is shown as the red dot. Lower panel: sky map for the BOAV station showing the distribution of Faraday rotation angle due to ionosphere. The dotted lines and the dot show possible trajectories and instantaneous position of the communication satellite as shown in the upper panel.

two regions of strong positive increment in the polarization angle can be observed in the North-East and North-West directions, cf. Fig. 4 (lower panel). This enhancement is due to the ionization crest located over and northwards of the BOAV station. In the other part of the sky, the zero or negative values of the FR angles can be seen close to the horizon. This is due to the smaller ionospheric electron density in the region of magnetic equator that is situated southwards of the BOAV station. It is worth to note that since the GISM is a climatological model, the calculated values of the FR are primarily applicable for quiet space weather conditions only and excludes the detailed analysis of the extreme events such as presented in Fig. 3. In the present article the storm condition is then incorporated by choosing the highest level for the solar radio flux of 140 sfu measured during this period. As the solar flux is the driving parameter of the GISM, the enhanced scintillation activity due to the storm is thus included in the following considerations. On the other hand, we omit any consideration of storm-associated disturbances of the geomagnetic field.

In the simulation of communication scenario between the BOAV station and the AlfaCrux satellite we see that in total four communication links could be established during this particular day with one passage during the time slot of interest. The instantaneous position of the satellite is shown as the red dot on the sky plot. During this satellite passage the FR increment changes from negative to large positive value reaching northwards the region of disrupted communication channel if linearly-polarized receiver antenna is used.

3) MITIGATION OF POLARIZATION LOSS FACTOR

As presented in the previous section, the attenuation due to FR can be significantly high depending on the type of polarization used in the receiver and transmitter antennas. Therefore, power loss due to FR and associated depolarization has to be taken into account for the link budget computation. The latter is the comparison between the power given to the transmitter, the amount of power available in the receiver and the noise level at the same point of the receiver [1]. In case when the depolarization is well estimated, linearly polarized antennas may be employed on the ground station and adjusted to compensate the depolarization effect. Unfortunately, due to the short periods of satellites visibility (a few minutes at each passage), the FR must be quickly estimated, and the antenna must be quickly adjusted so the polarization losses may be reduced [11]. This can be a challenging and costly task due to the high variability of the ionosphere in certain times and locations.

Based on the variability of the FR presented in this study, is was defined as the most suitable solution for dealing with the depolarization effects on the AlfaCrux mission the use of turnstile antenna with circular polarization on the satellite. At the ground station, two X-Quad antennas (2×18 elements) with gain of 14.95 dBi, being one right-hand circular polarized (RHCP) and the other left-hand circular polarized (LHCP) are being used. In order to increase the link connection, the ground station was designed using a diversity scheme. The latter uses the two outputs of the antennas to obtain the signal from ever possible polarization of the incident wave [1], [21]. The polarization loss estimated with such approach is around 1 dB, which corresponds to 2 dB less then the maximum loss expected when using a circular polarized antenna at the satellite and a linear one at the ground station [22].

B. IONOSPHERIC SCINTILLATION

The presence of ionospheric plasma irregularities, with scales varying from centimeter to hundred of kilometers, can cause fluctuations on the refractive index of the medium which lead to rapid random modulation of the amplitude and phase of the trans-ionospheric signal. This phenomena,

called scintillation, is one of the most severe disruptions on trans-ionospheric signals with frequency below 3 GHz [18]. In the equatorial regions, it is well known that this phenomenon is likely to occur during post-sunset hours, with enhanced activity during equinoxes [19]. With this in mind, the purpose of this investigation is to quantify and characterize the average values of scintillation levels over the Brazilian region in order to support the mission and to propose a methodology for evaluating the risk of communication disruption during scintillation periods.

Two indices are usually employed to characterize the amplitude and phase scintillation levels: the S_4 and σ_ϕ indices, respectively. The former index is defined as the standard deviation of the normalized signal power over a determined period and usually can be classified in three levels: weak ($S_4 < 0.3$), moderate ($0.3 \leq S_4 \leq 0.6$) and severe ($S_4 > 0.6$). For weak and moderate regimes, most observations in equatorial regions indicate that phase and intensity scintillation are strongly correlated [18]. Therefore in this study we focus on the amplitude scintillation index S_4, which can be calculated according to:

$$S_4 = \sqrt{\frac{\langle I^2 \rangle - \langle I \rangle^2}{\langle I \rangle^2}}. \tag{3}$$

Here I corresponds to the signal intensity (which is proportional to the square of the signal amplitude) and $\langle \ldots \rangle$ denotes either the ensemble or time averaging under the assumption that the received intensity is an ergodic random process [18], [23].

In order to investigate the scintillation effects on UHF satellite communication systems, we have used again the GISM model which is the model recommended by the International Telecommunications Union (ITU) for ionospheric scintillation intensity prediction. This model has been validated in multiple studies and suits well for estimation of scintillation levels for navigation and telecommunication purposes. The ionosphere electron density at any point of the modeled medium is obtained from the NeQuick model [24], which is also included in the GISM [19]. As the solar irradiance is one of the driving parameters of the NeQuick model, the scintillation indices calculated with the GISM are sensitive to this parameter as well.

In order to investigate the occurrence of scintillation over the Brazilian region, we use the CUIB and BOAV stations to perform the simulations using the GISM. These particular stations are selected due to their close location to the south and north crest of the Ionospheric Equatorial Anomaly (IEA), respectively, which are areas where one can expect the occurrence of scintillation [25]. The locations of these stations are shown in Fig. 4, upper panel. They are part of the Brazilian Network for Continuous Monitoring (RBMC) and are maintained by the Brazilian Institute for Geography and Statistics.

For each one of the aforementioned locations, the S_4 index was calculated using the GISM for the year of 2017. Fig. 5

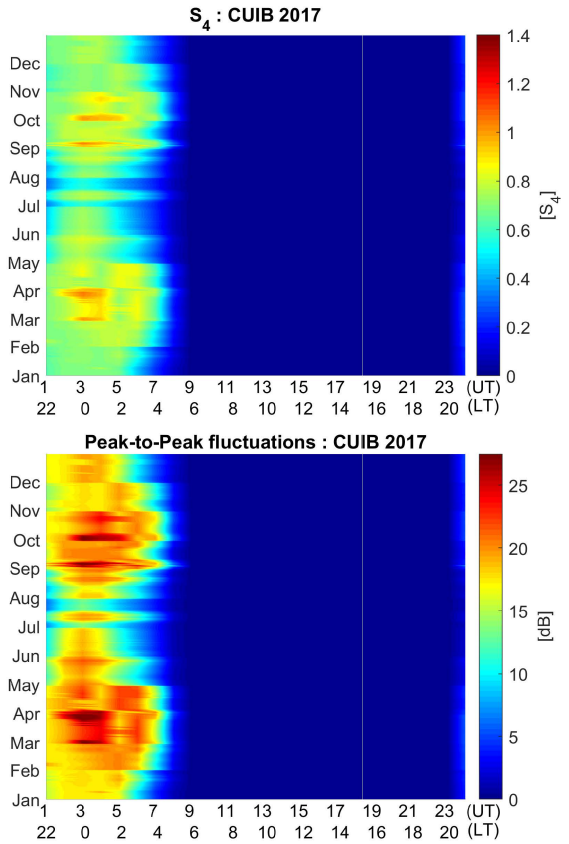

FIGURE 5. S_4 scintillation index (upper panel) and estimated signal peak-to-peak fluctuations (lower panel) for the CUIB station during the year 2017 for a 437MHz signal.

(upper panel) presents the scintillation index for the CUIB as a function of local time and day of the year. One can note, that significant levels of the S_4 index are observed during the equinoxes. Also during these periods, one can observe that such levels can last up to 5:00 LT (8:00 UT).

In order to verify the level of peak-to-peak fluctuations of the signal associated with the observed S_4 levels, one may use the following empirical relation [18]:

$$\mathcal{P}_{fluc}[dB] = 27.5\, S_4^{1.26}. \tag{4}$$

Based on this formula, the results for the CUIB station are computed and presented Fig. 5 (lower panel), indicating significant levels of peak-to-peak fluctuation during the post-sunset hours, reaching values higher than 25 dB.

Fig. 6 presents the level of scintillation throughout the day and how it varies seasonally for the CUIB location. It shows the frequency of occurrence of different scintillation levels for each season of the year 2017 as a function of local time. One can note that during all seasons, severe levels of scintillation are expected between 22:00 and 4:00 LT, with higher levels observed during summer and lower levels observed during the winter of 2017. Moderate values, on the other hand, are observed more frequently during the winter and less frequently during the summer. During the autumn and spring, similar frequencies of occurrence were observed with the

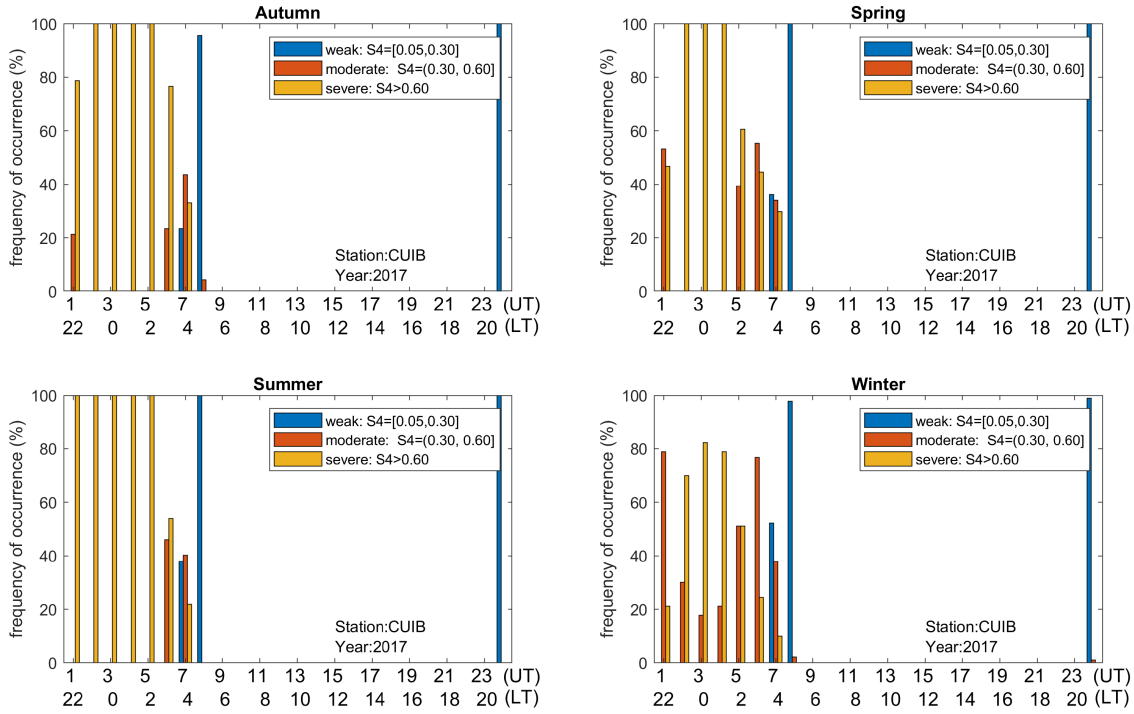

FIGURE 6. Percentage of occurrence of the signal fluctuation levels for the CUIB station for different seasons of the year 2017.

slightly higher occurrence of severe scintillation during the autumn when compared to the spring.

Aiming at investigating the latitudinal variability of the scintillation over the Brazilian sector, we have conducted similar analysis for the BOAV location. Fig. 7 (upper panel) shows the S_4 index as a function of local time and day of the year. One can note that the S_4 levels for this location are significantly lower than those observed at CUIB. Moderate levels of scintillation, that are observed to occur up to 5:00 LT for the CUIB station, are in the case of the BOAV mostly restricted to the interval from 23:00 to 4:00 LT. The levels of peak-to-peak fluctuations presented in Fig. 7 (lower panel) exhibit notably lower values, when compared to the CUIB station, except for some periods, such as the September 2017 events. From Fig. 8 one can infer that severe levels of scintillation for this location are not very frequently observed, being mostly restricted to the interval from 23:00 and 3:00 LT and more often observed during winter and spring.

The comparison of different regions of the Brazilian sector exhibits the variability of scintillation levels on the geographic location. Thus, such spatial variability has to be taken into consideration when designing a satellite communication service, such as the AlfaCrux mission. The analysis shows that considerable levels of peak-to-peak fluctuations due to scintillation for the signals on the 437 MHz frequency can occur. Such levels might compromise the communication reliability during the post-sunset hours, and depending on the application, can jeopardize the communication tasks. Different cases illustrate situations in which the scintillation can compromise narrowband communication [22], leading to the complete interruption of the link in some extreme cases. An example of such communication outage has been reported during the Anaconda operation [26], when the tactical communication failed due to extensive scintillation and multi-path effects. Therefore, for the mission planning of a communication satellite it is important to investigate quantitatively how much such scintillation can impact the reliability and performance of the communication link. The next section presents the results in this regard.

III. SCINTILLATION AND COMMUNICATION RESILIENCE

The communication planning for the AlfaCrux mission takes into account the scintillation effects on the satellite signal by means of the S_4 index derived from the GISM. Based on the level of peak-to-peak fluctuation of the signal associated with the observed S_4 index, one can estimate the correspondent signal loss to be accounted in the link budget computation. The signal loss associated with scintillation can be expressed as

$$L_{fluc} = \frac{\mathcal{P}_{fluc}}{\sqrt{2}}, \tag{5}$$

where $\mathcal{P}_{fluc}$ is given by (4) and correspond to the peak-to-peak fluctuation in dB [18].

Although the scintillation effects are intense in the equatorial regions, the impacts on the communication missions are frequently overlooked on the link budget computation [26]. Henceforth, it is necessary to develop a methodology for including the scintillation effects on the planing of the communication link of space missions. More specifically,

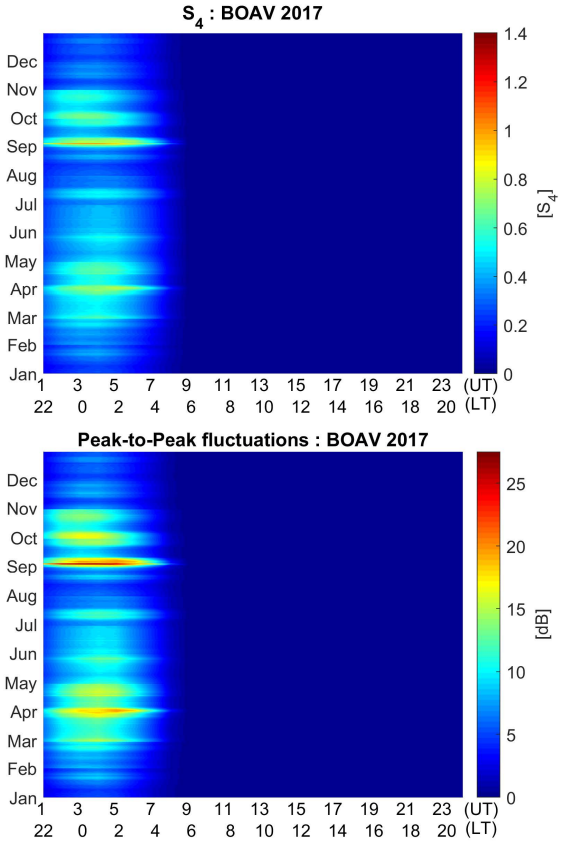

FIGURE 7. S_4 scintillation index (upper panel) and estimated signal peak-to-peak fluctuations (lower panel) for the BOAV station during the year 2017 and for a 437MHz signal.

the mapping of the communication channel availability in regions exposed to strong scintillation is of great practical importance in this case. Based on this method, we assess the risk of communication loss caused by scintillation. Additionally to this, we indicate the most favorable time intervals and regions for communication, even during periods of expected scintillation over the Brazilian sector.

A. RISK ANALYSIS

The usage plan for the communication channel proposed in this work is based on the risk analysis from the decision theory [27], [28]. In this context, given a specific activity (e.g. satellite-receiver communication), one can define the risk as the expected loss incurred to such activity. In order to estimate the risk it is necessary [28]:

- to find features that describe the condition in which the activity is performed (e.g. S_4 level can describe communication under scintillation);
- to determine the frequency of occurrence of such features;
- to know how injurious the condition described by these features is for the successful outcome of activity.

Each of these requirements can be expressed by a feature vector, a probability and a loss function, respectively. Denoting random variables by capital letters and their realizations by lower-case letters, one can start with the measurable variable feature $Z \in \mathcal{Z}$, where $\mathcal{Z}$ represents the set of all possible feature vectors. In order to illustrate the concept, one can consider the indicator function (also called the loss function), given by

$$l(z; z_{thr}) = \begin{cases} 0, & \text{if} \quad z < z_{thr}, \\ 1, & \text{otherwise}, \end{cases} \tag{6}$$

which suggest that there is no loss when values of z are below a threshold value z_{thr}. In the case $z \geq z_{thr}$, losses are equally injurious [28]. The risk $r(z_{thr})$ is defined as the expected value of the indicator function presented in (6), and is given by

$$r(z_{thr}) = \langle l(z; z_{thr}) \rangle = \int_{\mathcal{Z}} l(z; z_{thr}) p(z) dz = \pi(Z \geq z_{thr}), \tag{7}$$

where $p(z)$ is the probability density function of the feature Z, and $\pi(Z)$ corresponds to the probability function. In such way, the risk has an interpretation in terms of the probability. Based on the risk concept in combination with the analysis of the link budget we investigate how the scintillation might impact the communication activities.

B. LINK BUDGET

The link budget is estimated by comparing the power given to the transmitter to the power available at the receiver assuming that the transmitted signal is exposed to the noisy environment along the propagation path. When a communication satellite is used, there are two different link budgets, the uplink (from the ground station to the satellite) and the downlink (from the satellite to the ground station) [1]. The power received by a real antenna can be expressed as [29], [30]:

$$P_r = \frac{P_t G_t G_r}{L_{t+r}} \quad [\text{W}], \tag{8}$$

where G_t and G_r correspond to the transmitter and receiver antennas gains, P_t corresponds to the transmitted power and L_{t+r} represents all losses, including losses due to attenuation in the atmosphere, losses associated with the transmitting and receiving antenna, polarization and free-space path losses [1], [3], [31]. In particular, the free-space loss depends on the propagation path length R as

$$\begin{aligned} L_{fs} &= (4\pi R/\lambda)^2, \\ R &= \sqrt{(R_\oplus + H)^2 - R_\oplus^2 \sin^2\theta_o} - R_\oplus \cos\theta_o, \end{aligned} \tag{9}$$

where λ is the signal wavelength, $R_\oplus$ is the Earth radius and H is the satellite altitude. At large zenith angles θ_o the free space loss becomes considerable for possible communication outage.

At the same time for simplicity we ignore the dependence of tropospheric loss on zenith angle as this loss level is considerably lower than the free-space one. In this investigation, we consider the attenuation due to rain and foliage as the main tropospheric losses. In the former case,

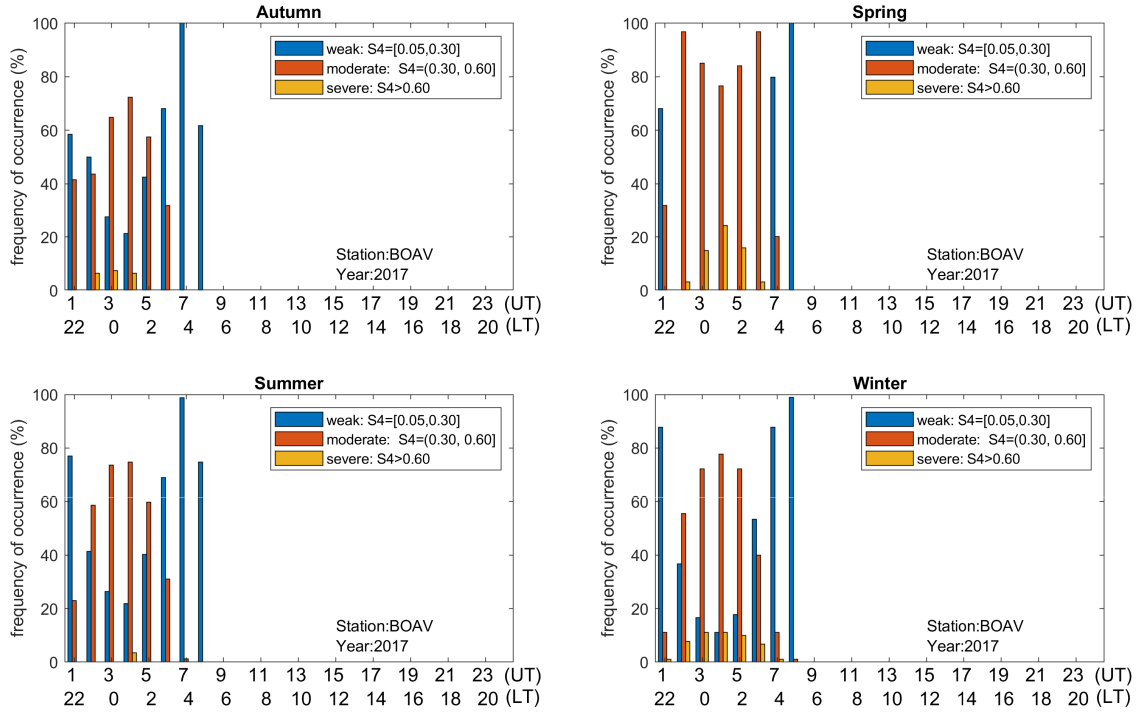

FIGURE 8. Percentage of occurrence of the signal fluctuation levels for the BOAV station for different seasons of the year 2017.

for the frequency of 437 MHz the attenuation estimated based on the recommendation ITU-R 837-7 [32] is lower than 0.001 dB only. For the latter, the attenuation estimates are obtained based on the model of attenuation due to foliage described in [33], considering an average foliage depth of 5 meters [34]. Combined, both effects lead to losses of approximately 3.3 dB.

For disturbed ionosphere, the loss L_{t+r} includes also the fluctuating losses in addition to the aforementioned regular losses. The fluctuating losses are associated primarily with the ionospheric scintillation and are described by the quantity L_{fluc}, cf. (5). The intermittent and intense space weather events also contribute to the enhancement of this contribution to the total loss budget.

The link budget, therefore, is a set of parameters that define the communication link in terms of power available for a reliable transmitter-receiver connection. Such link information is also useful to obtain the satellite-to-ground (downlink's) energy-per-bit to noise spectral density, which measures the reliability of the communication channel [3]. The energy-per-bit, E_b, to noise spectral density, N_o, at the ground station can be expressed as [30]

$$\frac{E_b}{N_o} = \frac{P_t G_t G_r}{L_{t+r} k T R_b}, \tag{10}$$

where T is the system temperature noise, R_b is the target data rate and $k = -228.6$ dB(W/K/Hz) is the Boltzmann constant.

Based on the communication requirements for the AlfaCrux mission, the link budget has been computed and is presented in Table 2, and the E_b/N_o and margin are obtained. In this study, we focus on the downlink for the AlfaCrux mission, since it provides a lower margin when compared to the uplink.

TABLE 2. Parameters of the link budget calculation for an elevation angle of 30°.

Parameter	Value
Frequency	437 MHz
Data rate (R_b)	9600 bps
Cubesat antenna gain (G_t)	0.0 dBi
Ground station antenna gain (G_r)	14.95 dBi
Transmitted power (P_t)	1 W (0 dbW)
Free-space loss	144.43 dB
Tropospheric loss	3.3 dB
Polarization loss	1.04 dB
Noise temperature (T)	500 K
E_b/N_o	27.95 dB
Required E_b/N_o	8.4 dB
Margin	**19.56 dB**

As presented in Table 2, the design of a satellite mission relies on the information of the required performance of the uplink and downlink, the propagation characteristics for the frequency band used, and the parameters of the satellite and the ground station. Sometimes, however, the complete information is not available and the designer must estimate values and generate tables of system performance based on assumed scenarios. Usually, the loss levels determined for the uplink and downlink depend on the signal frequency chosen by the designer, who in most cases shall also estimate the losses due to ionospheric attenuation on the link budget

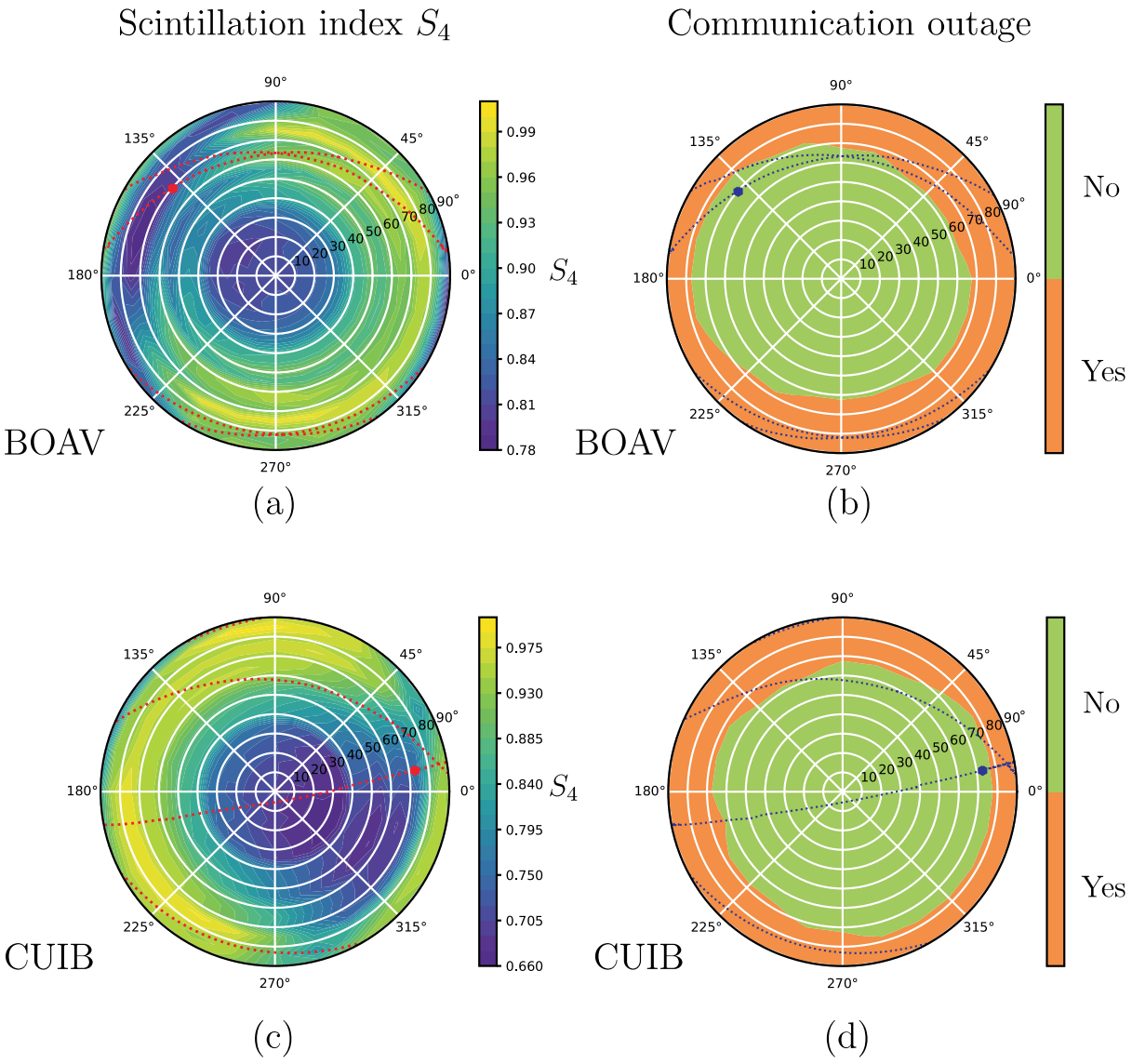

FIGURE 9. Scintillation S_4 indices (a), (c) and the associated communication outage maps (b), (d) mapped to the sky plots for the BOAV and CUIB ground stations. The maps are calculated for the period of high scintillation activity over the Brazilian region on 7th of September 2017 at 01:30 UT. The sample satellite passages during one day are also shown (dashed lines) with the instantaneous position of the satellite at 01:30 UT marked by a dot.

computation [31]. Fluctuating losses due to ionospheric scintillation often occur at UHF at the level of 2-3 dB peak-to-peak values, but can reach significant levels during occasions when steep ionospheric gradient densities are present. Such scintillation levels can reach as high as 27 dB [26], [35]. The associated fluctuating losses are not included in the margin computation presented in Table 2, however they need to be taken into account for low latitude regions, since signal fades of approximately 10 dB or higher, combined with other effects such as multipath, are sufficient to cause communication outages [26].

From the best knowledge of the authors, a systematic procedure aiming to optimize the planning of small satellite missions, such as AlfaCrux, is still missing. In this regard, it is desirable to have a metric that allows one to assess the probability of success on the communication during post-sunset hours in equatorial regions when the severe fluctuating loss due to scintillation may occur. In this sense, we propose a methodology that takes into account the attenuation due to scintillation on the computation of the link margin. Combining the scintillation level information with the risk analysis presented in Sec. III-A one can derive the risk of communication outage. Similarly to Sec. II-A2 we use thus the simulated TLE for calculation of the satellite Keplerian parameters, see Table 1. Scintillation level information and the corresponding communication outage regions are convenient to present as sky plots for specified receiving ground stations. Fig. 9 shows such plots with the superimposed possible satellite trajectories for the BOAV and CUIB stations.

Scintillation indices S_4 in Figs. 9 (a), (c) are calculated using the GISM for the 7th of September 2017 at 1:30 UT. This time corresponds to high scintillation activity in the Brazilian region. As the driving parameter of the model the 10.7 centimeter solar radio flux with value of 140 has been used. One can see that the scintillation index grows with the increase of the zenith angle. This effect is associated to the growing propagation path of the signal in the irregular ionosphere.

The calculations of S_4 index for the BOAV station show the region of high scintillation activity spreading northwards starting from the East up to the southwest direction, see Fig. 9 (a). This maximum is related to one of the ionization crests that for specified time is located over and northwards of the station. In the southwards direction scintillation levels are comparable or even less than those at the region near the zenith. This effect is related with the location of the magnetic equator southwards of the station, which is the region with lower background electron density. The distribution of the scintillation index for this station can be compared with the map for the Faraday rotation in Fig. 4 (b). In both cases the background electron density correlate with the values of the FR angle and of S_4.

Fig. 9 (c) shows the analogous sky map of S_4 index for the CUIB station. In this case, the station is located in the region of the south ionization crest, so the region of the enhanced scintillation activity is seen for slant propagation paths that cross the ionosphere within the region that is located southwards of the station from North-East up to West directions. On can also observe the small region of large scintillation in North-West direction that corresponds to the north ionization crest.

Figs. 9 (b) and (d) show the communication outage maps for the BOAV and CUIB stations. These maps are obtained after the inclusion in the link budget computation of the attenuation factor due to scintillation-associated fluctuating losses. In other words, based on the scintillation levels at each point of the sky maps in Figs. 9 (a), (c), a new energy-per-bit to noise spectral density ratio, $(E_b/N_o)_{scint}$, is computed and compared to the required ratio $(E_b/N_o)_{req}$. The required energy-per-bit to noise spectral density ratio is set by the mission requirements, whereas the ratio $(E_b/N_o)_{scint}$ is obtained from (10) with the inclusion of the signal loss factor given by (5). In the case when $(E_b/N_o)_{scint} < (E_b/N_o)_{req}$, an outage event is assumed to occur and corresponds to the *yes* region in Figs. 9 (b), (d). On the other hand, regions where the scintillation does not reduce E_b/N_o below the required levels are marked as *no* regions corresponding to no communication outage due to scintillation.

It can be observed that the regions of communication outage appear primarily at large zenith angles. The extension of these regions is closely related with the location of the ionization crests relative to the ground station at a specified time. This behaviour is similar to the above discussed regions of high scintillation activities for these stations. Another observation is that the communication outage is present at time of high scintillation activity for all azimuth angles if the zenith angle is greater than 80°. This is the cumulative effect of strong scintillation-associated loss and purely free-space loss. The latter depends on the length of the slant propagation path, that in turn becomes large for large zenith angles, see (9). This suggests to apply the masking angle of 10° for ground observers in the communication mission for AlfaCrux satellite for times of high scintillation activity. It can be seen that the fixed mask angle of 30° could eliminate the outage possibility completely. However, the choice of such angle might significantly reduce the possibility of establishing communication with the satellite. This is well illustrated in Fig. 9 (b), where the satellite, which instantaneous position is shown with the dot, could establish short communication link, which will be discarded if the ground station is operated with the masking angle fixed to 30°. It is thus advantageous to use the variable adaptive mask angle that can be defined using the boundary between *yes* and *no* regions on the communication outage maps similar to those of Fig. 9 (b), (d).

C. RISK OF COMMUNICATION OUTAGE ASSOCIATED WITH SCINTILLATION

The scintillation-associated condition $(E_b/N_o)_{scint} < (E_b/N_o)_{req}$ for communication outage considered above can be utilized for the definition of the threshold value z_{thr} used in the risk analysis, as outlined in Sec. III-A. For that we define the random variable

$$z = |I - \langle I \rangle| / \langle I \rangle, \tag{11}$$

which is the normalized error for received signal intensity. The average intensity here can be calculated, for example, by accumulating measurements during some short time interval. Then the threshold z_{thr} is the maximal tolerable value of this quantity for which the communication is still possible. As this threshold is a number, one can interpret it as the minimally tolerable scintillation index S_4 [28].

Using (6) we define the loss function $l(z; z_{thr})$ that after averaging yields the required risk function of the communication outage $r_{outage} = \langle l(x; x_{thr}) \rangle$. The values of the risk function lie in the range [0, 1] with the highest risk value equal to one. This formula can be implemented in simulation programs as follows: scintillation simulating models are usually using the single- or multiple-phase screen algorithm. The idea behind this technique is that the properly generated phase screen placed within the ionospheric layer and along the propagation of a signal wave introduces random modulation of the phase of the latter. These gained random phase increments result in the formation complex diffraction pattern on the ground and in uneven distribution of received intensity. The single realization of the variable z corresponds to a single generation of a set of random phase screens along the propagation path. For the same communication geometry one then generate the set of random phase screens multiple number of times, then calculates the loss function $l(z; z_{thr})$ for each realization and perform the averaging in order to estimate the risk function.

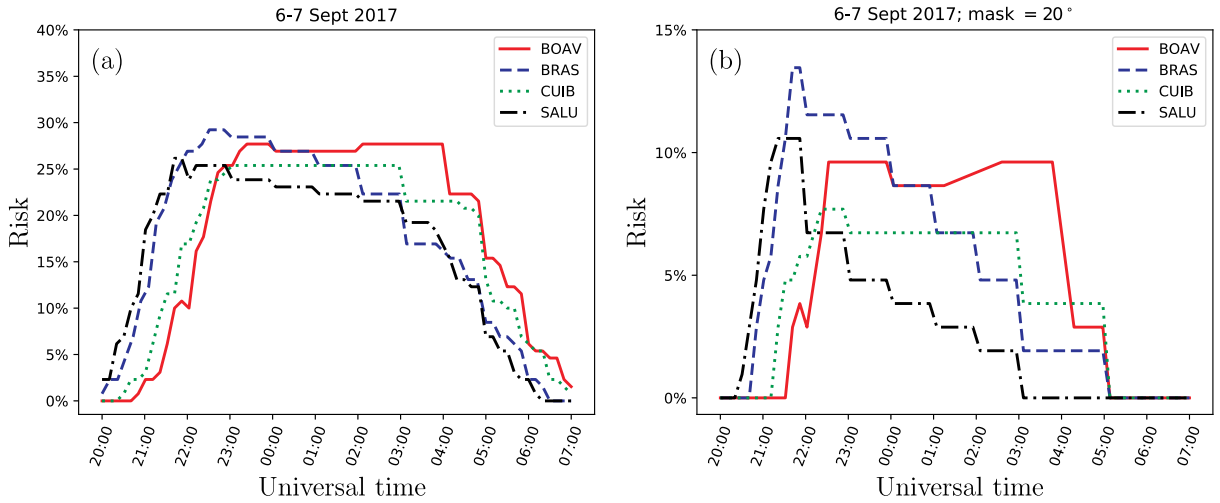

FIGURE 10. Risk of communication outage due to scintillation for the AlfaCrux mission for the cases when the ground stations establish communication without (a) and with (b) applying the mask angle of 20°. The curves are calculated for the equivalent isotropic radiated power of 1 W and the required energy-per-bit to noise spectral density ratio $(E_b/N_o)_{req} = 8.4$ dB.

Algorithm 1 Risk of Scintillation Impact on Low-Latitude SATCOM

Input: S_4 index
Output: Risk of communication outage
if -20°N ≤ Latitude ≤ 20°N **and** post-sunset LT **then**
  Compute the S_4 index for the area of interest;
  $P_{fluc} = 27.5S_4^{1.26}$;
  $L_p = \frac{1}{\sqrt{2}}P_{fluc}$;
  Include attenuation due to scint. (L_p) in the link budget;
  Compute $(E_b/N_o)_{new}$;
  if $(E_b/N_o)_{new} > (E_b/N_o)_{req}$ **then**
    Satisfactory link margin
    Communication channel available
  else
    Communication channel not available;
  end if
  Compute risk: The ratio of the interest region (sky plot) with communication outage to the total area
else
  Low risk of scintillation impact on the channel (channel available)
end if

In the view that the scintillation simulation programs, such as the GISM, provide just the interface for calculating the scintillation index S_4 alone, it is reasonable to adjust the aforementioned calculation procedure. We use then the empirical relation (4) along with (5) for estimation of the communication outage risks. In particular, the calculated fluctuating loss (5) is used in the total loss budget L_{t+r} and then the ratio (10) is calculated. This estimated energy-per-bit to noise spectral density ratio $(E_b/N_o)_{scint}$ is compared with the required value $(E_b/N_o)_{req}$ and the communication outage map is constructed in the similar manner as shown in Fig. 9 (b) and (c). The evaluation of the risk function (7) is performed than by geometric interpretation of the communication outage frequency as the ratio of sky map region with communication outage [orange area in Figs. 9 (b), (c)] to the total area (orange and green areas on the figure).

The algorithm 1 summarizes the procedure for doing this estimation. Fig. 10 presents the calculated risk for the BOAV, BRAS, CUIB, and SALU receiver stations as a function of the universal time for the night of 6-7th of September 2017. Fig. 10 (a) shows the risk if the whole sky hemisphere is used in the calculation, whereas Fig. 10 (b) show the risk curves if the mask angle of 20° is applied by ground stations. Since the zenith angles in the latter case are restricted to the range [0°, 70°], the estimated risk is clearly lower, however, in the expense of discarding some portions of sky where communication might still be possible.

Inspecting Fig. 10 one can note the dependence of shape and definition domain of the risk curves on the geographical location of the stations. The onset of the growing risk of communication outage for the BRAS and SALU stations is earlier than for the BOAV and CUIB stations since the former are located eastwards from the latter ones. Thus, the day/night terminator and the resulting onset of scintillation activity reaches the stations BRAS and SALU earlier than the BOAV and CUIB locations, cf. Fig. 4. The apparent skewness of the risk distribution for the SALU and the BRAS stations is related with the time evolution of the ionization crests at these longitudes.

Finally, we note that the risk calculated for the whole sky hemisphere as presented in Fig. 10 can be considered as the worst-case scenario risk estimation. As we have mentioned already, the usage of the 10° mask angle for post sunset times of high scintillation activity is a reasonable measure as for zenith angles larger than 80° the communication cannot be established. Using this mask angle in computation would

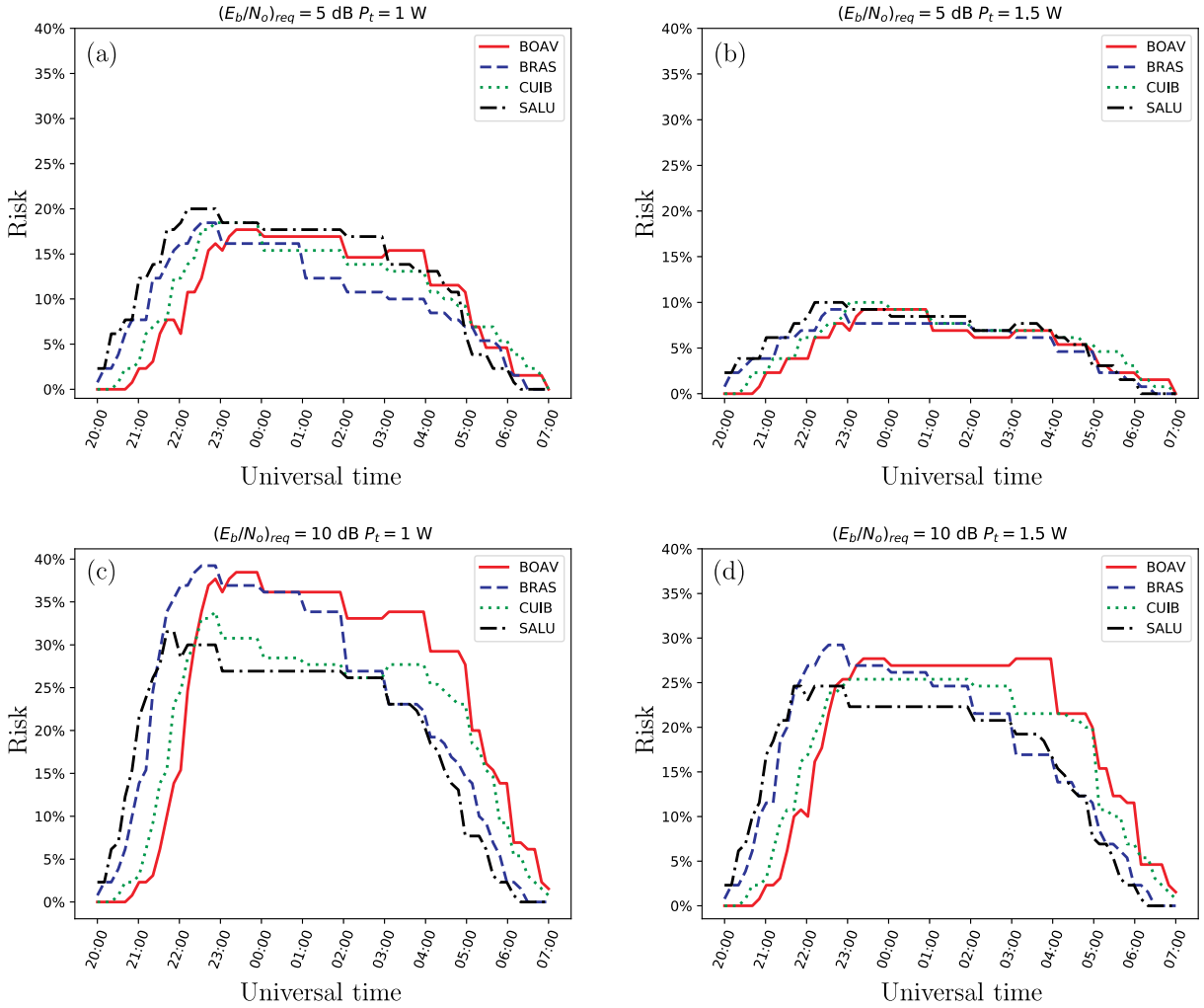

FIGURE 11. Evolution in time of the communication risk estimates for various values of the required threshold ratio $(E_b/N_o)_{req}$ and the power of the transmitter antenna. (a) $(E_b/N_o)_{req}$ = 5 dB and P_t = 1 W, (b) $(E_b/N_o)_{req}$ = 5 dB and P_t = 1.5 W, (c) $(E_b/N_o)_{req}$ = 10 dB and P_t = 1 W, (d) $(E_b/N_o)_{req}$ = 10 dB and P_t = 1.5 W. The calculations are performed for the night from 6th to 7th of September 2017 using the solar radio flux daytime value of 140 sfu.

reduce the risk level. However, we prefer to consider the risk analysis with no mask angle included as the intermittent space weather event might considerably influence the performance of communication missions. The considered here "worst-case scenario" provides some extra margin for possibility of space-weather-related signal disruptions in communication scenarios with finite mask angles of the ground receivers.

D. SCENARIOS EVALUATION

In this section different case studies are presented in order to demonstrate the capabilities of the proposed methodology to serve as a tool for the planning and operation of satellite communications in regions with high scintillation activity. In this set of simulations, the required values of $(E_b/N_o)_{req}$ are varied between 5 dB and 10 dB, and different values of transmitted power are chosen (1 W and 1.5 W). The reason for considering different values of transmitted power is motivated by the adaptive power control solution, in which the power of the transmitted signal is increased in order to compensate the attenuation along the signal propagation path. In such a case, under the favourable communication conditions, the transmitted power can be reduced, and when conditions deteriorate, transmitted power levels can be increased [36].

The results depicted in Fig. 11 show how the methodology can be used on the mission planning for the selection of the suitable transmitted signal power for the required E_b/N_o in order to reduce the probability of outage. These figures are calculated for the whole sky map coverage, i.e., zero mask angle, and can be considered as the worst-case scenario. Fig. 11 (a) and (c) can be compared with Fig. 10 (a) as plots for transmitter antenna with the same equivalent radiated power of 1 W, but with different values of the threshold value of $(E_b/N_o)_{req}$. It can be seen that the lowering the level of the required energy-per-bit to noise spectral density decreases the communication risk. Clearly, this dependence is because the level of the tolerable noise in the channel is accepted to be large.

On the other hand, if one compares the Figs. 11(a) and (b), or (c) and (d), the increase of the equivalent radiated power from 1 W to 1.5 W reduced the risk of communication outage. This occurs because the received energy P_r and, hence, the associated total energy-per-bit spectral density E_b are proportional to the antenna power P_t at the transmitter side, cf. Eqs (8), (10). The increase of these quantities relative to the fixed required value $(E_b/N_o)_{req}$ enlarges the threshold for channel loss level that can be tolerated and, therefore, reduces the associated communication risks. We also note that, since such small satellite missions as AlfaCrux have restriction on the payload weight and is thus limited in antenna transmitting power, the designers have to find an optimal compromise between the transmitted power and the acceptable communication performance.

IV. CONCLUSION

In this work, we analyze the effect of the ionosphere and different space weather phenomena on the UHF satellite communication systems and take the AlfaCrux UHF CubeSat mission as our case study. The level of absorbed solar ultraviolet energy by the atmosphere drives the ionization processes in the ionospheric layer. The resulting ionization levels have primarily the twofold effect on the radio communication systems operating in the lower UHF band.

Firstly, the propagating linearly-polarized signal from satellite experiences the action of the geomagnetic field. The latter rotates the polarization plane, an effect known as the Faraday rotation. The angle of rotation depends on the total electron content along the propagation path and, hence, on the background ionization level. If the linearly-polarized antenna is used for receiving the signal, the misalignment of the antenna polarization with the rotated polarization plane of the signal results into reduction or complete loss of the detected signal. For the AlfaCrux mission, the solution adopted to mitigate this problem consists on the use of a turnstile antenna with circular polarization on the satellite and a set of two X-Quad antennas for RCHP and LHCP at the ground station.

Secondly, the plasma that is lifted during the daytime diffuses downwards along the magnetic field lines forming two ionization crests situated on both sides of magnetic equator. At post-sunset hours, this process is accompanied by the formation of ionospheric instabilities, regions of depleted plasma and strong electron density gradients. The latter effects impact the phase and amplitude of the propagating signal wave in random manner, the phenomenon known as ionospheric scintillation. Similarly to the Faraday rotation effect, the strength of scintillation is related to the ionization levels, i.e., to the solar energy deposited in the ionosphere. For transient space weather events such as geomagnetic storms the ionization may be especially strong and the resulting scintillation may be especially severe.

In the present article we analyzed the morphology of the Faraday rotation angle, associated with its polarization loss factor, and the amplitude scintillation index for the UHF communication band. In particular, we investigated the variability of these quantities with the daytime, season, and geographic position for periods of low and high solar activity. For this task we considered the vertical communication link geometry that corresponds to the satellite position in zenith of ground-based receiver. In order to include the slant path effects in the analysis of communication disruptions we have used the sky plots for specified ground stations in Brazilian region. Such maps show the Faraday rotation angle and the scintillation index as functions of receiver's zenith and azimuth angles, incorporate the slant path effects and the refractive bending of signal rays, and show the trajectories and instantaneous position of the flying-by CubeSat. Additionally to this, the communication outage regions can be identified from such maps, which are useful for optimization of communication activity. For example, the border of communication outage region can be used for definition of the mask angle of the ground station in an adaptive way such that the communication link is closed if the satellite elevation angle is smaller than the determined mask angle.

We also present a new methodology to assess the risk of communication outage due to scintillation for the AlfaCrux mission. Such methodology can be used directly for different space missions operating in the UHF band. One can make use of already validated scintillation models for retrieving ionospheric scintillation information. By using climatological scintillation models such as the GISM, one can evaluate in advance the communication risks due to scintillation for specified receiver station and optimize the communication protocol. The risk level as a function of time serves well to this purpose. The dependence of such risks on the mission design parameters, such as the power or gain of transmitter antenna or the level of tolerable losses, gives an useful insight into the possible performance of the satellite communication mission and in a future step, we expect to validate the methodology on the real data collected from the AlfaCrux mission.

ACKNOWLEDGMENT

The authors would like to thank the Brazilian agencies CNPq and FAPDF which supported this work, and also the Brazilian Space Agency (AEB) and the Brazilian National Telecommunications Agency (ANATEL) for technical support and also would like to thank the use of NASA/GSFC's Space Physics Data Facility's OMNIWeb CDAWeb Service, OMNI data, and the Canadian Solar Monitoring Program database.

REFERENCES

[1] F. Aguado-Agelet, A. E. Villa, M. Arias-Acuña, and F. J. Díaz-Otero, "AOCS requirements and practical limitations for high-speed communications on small satellites," *Int. J. Aerosp. Eng.*, vol. 2019, pp. 1–16, Feb. 2019.

[2] O. Popescu, J. S. Harris, and D. C. Popescu, "Designing the communication sub-system for nanosatellite CubeSat missions: Operational and implementation perspectives," in *Proc. SoutheastCon*, Mar. 2016, pp. 1–5.

[3] N. Saeed, A. Elzanaty, H. Almorad, H. Dahrouj, T. Y. Al-Naffouri, and M.-S. Alouini, "CubeSat communications: Recent advances and future challenges," *IEEE Commun. Surveys Tuts.*, vol. 22, no. 3, pp. 1839–1862, 3rd Quart., 2020.
[4] L. R. Reis, R. A. Borges, J. P. Leite, C. Cappelleti, and S. Battistini, "An overview of the AlfaCrux CubeSat mission for narrowband communication," *Adv. Astron. Sci.*, vol. 173, pp. 245–255.
[5] E. Gündüzhan and K. D. Brown, "Narrowband satellite communications: Challenges and emerging solutions," *Johns Hopkins APL Tech. Dig.*, vol. 33, no. 1, pp. 52–56, 2015. [Online]. Available: https://www.jhuapl.edu/Content/techdigest/pdf/V33-N01/33-01-Gunduzhan.pdf
[6] E. R. de Paula, F. S. Rodrigues, K. N. Iyer, I. J. Kantor, M. A. Abdu, P. M. Kintner, B. M. Ledvina, and H. Kil, "Equatorial anomaly effects on GPS scintillations in Brazil," *Adv. Space Res.*, vol. 31, no. 3, pp. 749–754, Jan. 2003.
[7] J. H. A. Sobral, M. A. Abdu, H. Takahashi, M. J. Taylor, E. R. de Paula, C. J. Zamlutti, M. G. de Aquino, and G. L. Borba, "Ionospheric plasma bubble climatology over Brazil based on 22 years (1977–1998) of airglow observations," *J. Atmos. Solar-Terr. Phys.*, vol. 64, nos. 12–14, pp. 1517–1524, Aug. 2002.
[8] C. Nieto-Peroy and M. R. Emami, "CubeSat mission: From design to operation," *Appl. Sci.*, vol. 9, no. 15, pp. 1–24, 2019.
[9] W. Bothmer and J. A. Daglis, *Space Weather: Physics and Effects*, 1st ed. Berlin, Germany: Springer, 2007.
[10] G. S. Bust, W. Liles, and C. Mitchell, "Space weather influences on HF, UHF, and VHF radio propagation," in *Space Weather Effects and Applications*, A. J. Coster, P. J. Erickson, L. J. Lanzerotti, Y. Zhang, and L. J. Paxton, Eds. Washington, DC, USA: American Geophysical Union (AGU), 2021, ch. 7, pp. 153–163.
[11] D. Barbaric, J. Vukovic, and D. Babic, "Link budget analysis for a proposed cubesat Earth observation mission," in *Proc. 41st Int. Conv. Inf. Commun. Technol., Electron. Microelectron. (MIPRO)*, May 2018, pp. 0133–0138.
[12] M. Jehle, M. Rüegg, D. Small, E. Meier, and D. Nüesch, "Estimation of ionospheric TEC and Faraday rotation for L-band SAR," *Proc. SPIE*, vol. 5979, pp. 252–260, Oct. 2005.
[13] M. Singh and M. H. Bettenhausen, "An accurate and efficient algorithm for Faraday rotation corrections for spaceborne microwave radiometers," *Radio Sci.*, vol. 46, no. 4, pp. 1–16, 2011.
[14] R. S. Lawrence, C. G. Little, and H. J. A. Chivers, "A survey of ionospheric effects upon earth-space radio propagation," *Proc. IEEE*, vol. 52, no. 1, pp. 4–27, Jan. 1964.
[15] P. A. Wright, S. Quegan, N. S. Wheadon, and C. D. Hall, "Faraday rotation effects on L-band spaceborne SAR data," *IEEE Trans. Geosci. Remote Sens.*, vol. 41, no. 12, pp. 2735–2744, Dec. 2003.
[16] R. Galuscak and P. Hazdra, "Circular polarization and polarization losses," in *Proc. DuBus*, 2006, pp. 8–23.
[17] D. Oberoi and C. J. Lonsdale, "Media responsible for Faraday rotation: A review," *Radio Sci.*, vol. 47, no. 6, pp. 1–11, 2012.
[18] *Ionospheric Propagation Data and Prediction Methods Required for the Design of Satellite Networks and Systems*, document ITU, Recommendation ITU-R P.531-14, International Telecommunications Union, Geneva, Switzerland, Tech. Rep., 2019.
[19] Y. Béniguel and P. Hamel, "A global ionosphere scintillation propagation model for equatorial regions," *J. Space Weather Space Climate*, vol. 1, no. 1, p. A04, 2011.
[20] Y. Béniguel, "Ionospheric scintillations: Indices and modelling," *Radio Sci.*, vol. 54, no. 7, pp. 618–632, Jul. 2019.
[21] A. J. Vazquez-Alvarez, R. Tubio-Pardavila, A. Gonzalez-Muino, F. Aguado-Agelet, M. Arias-Acuna, and J. A. Vilan-Vilan, "Design of a polarization diversity system for ground stations of CubeSat space systems," *IEEE Antennas Wireless Propag. Lett.*, vol. 11, pp. 917–920, 2012.
[22] L. Fernandez, J. A. Ruiz-De-Azua, A. Calveras, and A. Camps, "Assessing Lora for satellite-to-earth communications considering the impact of ionospheric scintillation," *IEEE Access*, vol. 8, pp. 165570–165582, 2020.
[23] K. Guo, M. Aquino, and S. V. Veettil, "Ionospheric scintillation intensity fading characteristics and GPS receiver tracking performance at low latitudes," *GPS Solutions*, vol. 23, no. 2, pp. 1–12, Apr. 2019.
[24] S. M. Radicella, "The NeQuick model genesis, uses and evolution," *Ann. Geophys.*, vol. 52, nos. 3–4, pp. 417–422, Jun. 2009.
[25] E. Correia, M. T. A. H. Muella, L. Alfonsi, F. S. P. Prol, and P. O. Camargo, *Accuracy GNSS Methods*. London, U.K.: IntechOpen, 2018, ch. GPS Scintillations and Total Electron Content Climatology in the Southern American Sector.
[26] M. A. Kelly, J. M. Comberiate, E. S. Miller, and L. J. Paxton, "Progress toward forecasting of space weather effects on UHF SATCOM after operation anaconda," *Space Weather*, vol. 12, no. 10, pp. 601–611, Oct. 2014.
[27] S. Oppe, "The concept of risk: A decision theoretic approach," *Ergonomics*, vol. 31, no. 4, pp. 435–440, Apr. 1988.
[28] A. Koulouri, N. D. Smith, B. C. Vani, V. Rimpiläinen, I. Astin, and B. Forte, "Methodology to estimate ionospheric scintillation risk maps and their contribution to position dilution of precision on the ground," *J. Geodesy*, vol. 94, no. 2, pp. 1–22, Feb. 2020.
[29] F. T. Ulaby, R. K. Moore, and A. K. Fung, *Microwave Remote Sensing. Active and Passive*, vol. 1, 1st ed. Reading, MA, USA: Addison-Wesley, 1981.
[30] J. R. Wertz and W. J. Larson, *Space Mission Analysis and Design*, 3rd ed. Dordrecht, The Netherlands: Kluwer, 1999.
[31] T. Pratt and J. Allnutt, *Satellite Communications*, 3rd ed. Hoboken, NJ, USA: Wiley, 2020.
[32] *Characteristics of Precipitation for Propagation Modelling*, document ITU, Recommendation ITU-R P.837-7, International Telecommunications Union, Geneva, Tech. Rep., 2017.
[33] Z. Hasirci, I. H. Cavdar, and M. Ozturk, "Single tree vegetation depth estimation tool for satellite services link design," *Radioengineering*, vol. 25, no. 1, pp. 140–147, Apr. 2016.
[34] I. A. Hemadeh, K. Satyanarayana, M. El-Hajjar, and L. Hanzo, "Millimeter-wave communications: Physical channel models, design considerations, antenna constructions, and link-budget," *IEEE Commun. Surveys Tuts.*, vol. 20, no. 2, pp. 870–913, 2nd Quart., 2018.
[35] S. Basu, J. P. McClure, S. Basu, W. B. Hanson, and J. Aarons, "Coordinated study of equatorial scintillation and *in situ* and radar observations of nighttimeFregion irregularities," *J. Geophys. Res., Space Phys.*, vol. 85, no. A10, pp. 5119–5130, Oct. 1980.
[36] D. R. Glover, "Satellite radio communications fundamentals and link budgets," in *Handbook of Satellite Appl.*, 2nd ed., J. N. Pelton, S. Madry, and S. Camacho-Lara, Eds. Cham, Switzerland: Springer, 2017, pp. 431–462.

A. A. FERREIRA (Member, IEEE) received the B.S. degree in electrical engineering and the M.Sc. degree in electronic and automation systems engineering from the University of Brasília (UnB), in 2013 and 2018, respectively, where he is currently pursuing the Ph.D. degree in electrical engineering. Since 2018, he has been conducting his research with the German Aerospace Center (DLR), Department for Solar-Terrestrial Coupling Processes, jointly with the Laboratory for Simulation and Control of Aerospace Systems (LODESTAR, UnB). His research interests include ionospheric modeling, space weather and its impacts on the ionosphere and satellite communication, nonlinear systems, machine learning, and global navigation satellite systems.

R. A. BORGES (Senior Member, IEEE) received the master's and Ph.D. degrees in electrical engineering from the University of Campinas, in 2004 and 2009, respectively, and the Ph.D. degree in electrical engineering from the University of New Mexico, USA. From 2009 to 2011, he held a postdoctoral fellowship from the state of São Paulo Research Foundation working with the School of Electrical and Computer Engineering, University of Campinas. He is currently an Associate Professor with the Electrical Engineering Department, University of Brasília, and a Control System Researcher affiliated with the Laboratory of Automation and Robotics (LARA) and the Creator and a current Coordinator of the Laboratory for Simulation and Control of Aerospace Systems (LODESTAR), University of Brasília. He was the Head of the Electrical Engineering Department, from February 2018 to July 2020. Currently, he is the Coordinator of the first CubeSat mission for narrowband communication financed by the Government of the Federal District, Brazil. His research interests include Lyapunov stability theory of dynamic systems, modeling and control of rotating body, robust control, CubeSat ADCS, and development of high altitude scientific platforms. He is affiliated with the IEEE Aerospace and Electric Systems Society.

L. R. REIS received the B.Sc. degree in electrical engineering from the University of Mackenzie, São Paulo, Brazil, in 2009, and the M.Sc. degree in electronics and automation systems engineering from the University of Brasília, Brazil, in 2021. Currently, he is a member of Technical Staff of the Brazilian Space Agency (AEB), acting also as the substitute Coordinator of Policies and Programs (CPP) in the Space Sector Governance Directorate (DGSE). His research interests include space mission analysis and space weather impacts on satellite communication.

C. BORRIES received the Diploma degree in geoinformation from the University of Applied Sciences in Neubrandenburg, Germany, and the Ph.D. degree from the Free University Berlin, in 2011. From 2005 to 2011, she conducted her Ph.D. work with the German Aerospace Center (DLR) studying the signatures of planetary waves in the ionosphere. Following, her research focus were the effects of ionospheric storms in mid-latitudes. In 2015, she received a grant to build-up a young academics group at DLR. In parallel to leading this research group, she was acting in the period (2015–2021) in the ESA Space Weather Network as a Coordinator of the Ionosphere Expert Service Centre. Since 2019, she has been the Head of the Department for Solar-Terrestrial Coupling Processes in DLR, Institute for Solar-Terrestrial Physics in Neustrelitz, Germany. She works with her team in the analysis of thermosphere-ionosphere coupling with processes from above (magnetosphere and solar wind) and from below (atmospheric waves). Her research interests include studying thermosphere-ionosphere perturbations during storm conditions, such as storm enhanced densities and travelling ionospheric disturbances.

D. VASYLYEV received the master's and Ph.D. degrees in theoretical physics from the University of Rostock, Germany, in 2004 and 2009, respectively. From 2009 to 2018, he was a Visiting Scientist with the University of Rostock, St. Andrews, U.K., and the Bogolyubov Institute of Theoretical Physics, Ukraine. Since 2019, he has been joining the DLR Institute for Solar-Terrestrial Physics, Germany. His research interests include the satellite-mediated free space optical and radiowave communication, tropospheric, and ionospheric scintillation quantum optics and quantum communication.